Evaluation of a concerted vs. sequential oxygen activation mechanism in α-ketoglutarate–dependent nonheme ferrous enzymes

Serra Goudarzi[a,1], Shyam R. Iyer[a,1], Jeffrey T. Babicz Jr[a], James J. Yan[a,b], Günther H. J. Peters[c], Hans E. M. Christensen[c], Britt Hedman[b], Keith O. Hodgson[a,b], and Edward I. Solomon[a,b,2]

[a]Department of Chemistry, Stanford University, Stanford, CA 94305; [b]Stanford Synchrotron Radiation Lightsource, Stanford Linear Accelerator Center (SLAC) National Accelerator Laboratory, Stanford University, Menlo Park, CA 94025; and [c]Department of Chemistry, Technical University of Denmark, 2800 Kgs. Lyngby, Denmark

Edited by Marcetta Y. Darensbourg, Texas A&M University, College Station, TX, and approved January 29, 2020 (received for review December 20, 2019)

Determining the requirements for efficient oxygen (O_2) activation is key to understanding how enzymes maintain efficacy and mitigate unproductive, often detrimental reactivity. For the α-ketoglutarate (αKG)–dependent nonheme iron enzymes, both a concerted mechanism (both cofactor and substrate binding prior to reaction with O_2) and a sequential mechanism (cofactor binding and reaction with O_2 precede substrate binding) have been proposed. Deacetoxycephalosporin C synthase (DAOCS) is an αKG-dependent nonheme iron enzyme for which both of these mechanisms have been invoked to generate an intermediate that catalyzes oxidative ring expansion of penicillin substrates in cephalosporin biosynthesis. Spectroscopy shows that, in contrast to other αKG-dependent enzymes (which are six coordinate when only αKG is bound to the Fe^{II}), αKG binding to Fe^{II}-DAOCS results in ∼45% five-coordinate sites that selectively react with O_2 relative to the remaining six-coordinate sites. However, this reaction produces an Fe^{III} species that does not catalyze productive ring expansion. Alternatively, simultaneous αKG and substrate binding to Fe^{II}-DAOCS produces five-coordinate sites that rapidly react with O_2 to form an Fe^{IV}=O intermediate that then reacts with substrate to produce cephalosporin product. These results demonstrate that the concerted mechanism is operative in DAOCS and by extension, other nonheme iron enzymes.

oxygen activation | concerted mechanism | metalloenzymes | oxygenase chemistry

The oxygen (O_2)-activating mononuclear nonheme iron enzymes are important in antibiotic and neurotransmitter biosynthesis, hypoxia regulation, bioremediation, and DNA repair (1–7). They use a high-spin Fe^{II} site to activate O_2 to form iron–oxygen intermediates that transform a variety of organic substrates (8). These enzymes share a common 2-His/1-(Asp/Glu) facial triad motif to coordinate Fe^{II}, leaving three coordination positions for possible binding of O_2, cofactor (i.e., a source of additional electrons), and substrate (9). Using variable-temperature, variable-field magnetic circular dichroism (MCD) spectroscopy, we have shown that the nonheme iron enzymes utilize a general mechanistic strategy where the Fe^{II} site remains coordinatively saturated (i.e., no available site for O_2 activation) until both the cofactor and substrate are bound within the active site pocket. This ensures that the electron equivalents used to generate the iron–oxygen intermediate result in productive substrate oxidation (i.e., coupled turnover) (10).

A large subclass of the nonheme iron enzymes uses an α-ketoglutarate (αKG) cofactor as a source of two electrons for O_2 activation and has been shown to follow the general mechanistic strategy (11–13). The Fe^{II} resting sites are six coordinate, and the αKG cofactor coordinates to the Fe^{II} in a bidentate manner to form a site that remains six coordinate (12, 13). For this class of enzymes, substrates generally do not directly coordinate the Fe^{II} but rather, bind in the active site pocket, preserving a six-coordinate Fe^{II} site in the absence of αKG (14–16). However, simultaneous binding of αKG and substrate results in a coordinatively unsaturated five-coordinate Fe^{II} site that can now activate O_2 (11, 17). The O_2 reaction initiates oxidative decarboxylation of αKG (to form succinate and CO_2) to generate a reactive Fe^{IV}=O intermediate capable of substrate oxidation (18). This high-spin (S = 2) Fe^{IV}=O intermediate has been trapped in several αKG-dependent enzymes (19–22) and catalyzes a variety of chemical transformations initiated by a common hydrogen atom (H-atom) abstraction step from the substrate to form an Fe^{III}-OH and a substrate radical. Subsequently, the hydroxide (or a bound halide in the halogenases) can either rebound (resulting in hydroxylation/halogenation) or initiate a second H-atom abstraction (11) [or electron transfer (23, 24)], which leads to desaturation or ring closure/expansion (11, 18).

However, a sequential mechanism has alternatively been proposed in the literature to describe the O_2 reactivity of a number of nonheme iron enzymes (25–27) and was first proposed in deacetoxycephalosporin C synthase (DAOCS), an αKG-dependent enzyme important in the biosynthesis of cephalosporin antibiotics (2, 28, 29). DAOCS has broad substrate specificity, showing expandase activity on penicillins with different side chains, including penicillin-G (30). Unlike the other enzymes in the αKG subclass, crystallography on DAOCS showed

Significance

Many iron-dependent enzymes utilize molecular oxygen to functionalize inert C–H bonds in biology. Nonheme ferrous enzymes perform these reactions by reducing dioxygen, often in the presence of a sacrificial electron donor, to form a reactive intermediate that converts substrate to product. In α-ketoglutarate (αKG)–dependent enzymes, there has been discussion on the necessity of substrate prebinding to the αKG-bound ferrous center for productive chemistry. This study demonstrates that, when substrate is not prebound to the enzyme, the species generated in the reaction with dioxygen is not competent to perform hydrogen atom abstraction from the substrate. In contrast, when both cosubstrates are prebound to the enzyme, efficient coupling between dioxygen reduction and substrate oxidation is observed, leading to productive chemistry.

Author contributions: S.G., S.R.I., and E.I.S. designed research; S.G., S.R.I., J.T.B., J.J.Y., G.H.J.P., and H.E.M.C. performed research; S.G., S.R.I., J.T.B., J.J.Y., B.H., K.O.H., and E.I.S. analyzed data; and S.G., S.R.I., and E.I.S. wrote the paper.

The authors declare no competing interest.

This article is a PNAS Direct Submission.

[1]S.G. and S.R.I. contributed equally to this work.

[2]To whom correspondence may be addressed. Email: solomone@stanford.edu.

This article contains supporting information online at https://www.pnas.org/lookup/suppl/doi:10.1073/pnas.1922484117/-/DCSupplemental.

First published February 24, 2020.

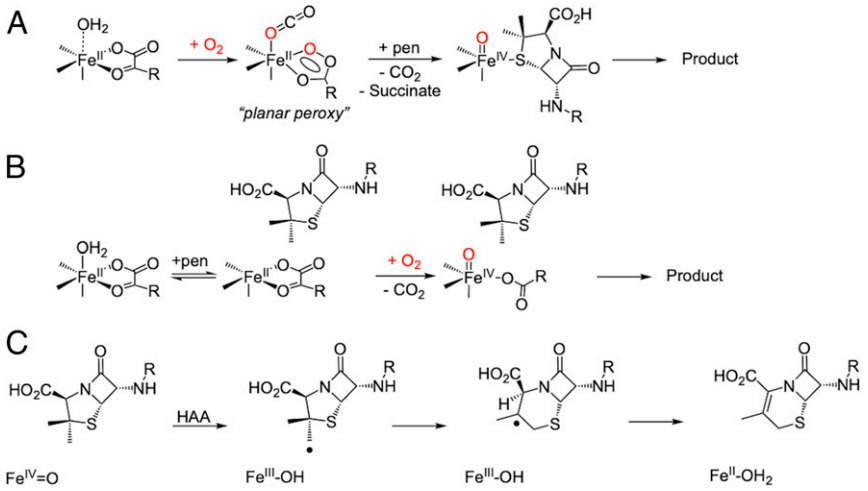

Scheme 1. (*A*) Sequential mechanism proposed for DAOCS. (*B*) Concerted reaction of the Fe^{II}/αKG/penicillin (pen) site with O_2. (*C*) Mechanism of DAOCS-catalyzed ring expansion, initiated by Fe^{IV}=O catalyzed H-atom abstraction (HAA).

penicillin-G substrate coordinating directly to the Fe^{II} and did not observe simultaneous αKG and penicillin-G binding (25). These observations resulted in a proposed sequential mechanism (Scheme 1*A*) for DAOCS where 1) αKG first binds and then, the site reacts with O_2 to generate an intermediate that is stored in a ferrous "planar peroxy" form until 2) substrate binding results in the generation of an Fe^{IV}=O intermediate for the two-electron oxidative ring expansion. However, a recent mass spectrometry study provided evidence of simultaneous αKG and penicillin-G binding that supports the general mechanistic strategy (Scheme 1*B*) (31). Both mechanisms predict an Fe^{IV}=O intermediate, which initiates the ring expansion via H-atom abstraction from the β-methyl group of penicillin to form an Fe^{III}-OH and a methylene radical. This primary methylene radical is proposed to convert to a tertiary radical following ring expansion (Scheme 1*C*), which is thought to occur through a putative thiyl radical species. Subsequent reaction between the Fe^{III}-OH and tertiary radical gives the ring-expanded, desaturated product and Fe^{II}-OH_2 (32–34).

In order to determine whether some nonheme iron enzymes can function via a sequential mechanism, this study uses MCD spectroscopy to define the coordination environment of the Fe^{II} site in resting DAOCS and in its interactions with αKG cofactor and penicillin-G substrate. These studies have 1) identified a five-coordinate Fe^{II} component when only αKG is bound that selectively (relative to the six-coordinate Fe^{II}) reacts with O_2. 2) This reactivity enabled us to evaluate and eliminate the sequential mechanism. 3) Alternatively, when both αKG and penicillin-G are bound to DAOCS, we directly observe the Fe^{III} species formed after H-atom abstraction along with a substrate radical that decay together to form the cephalosporin product. This study confirms that ring expansion in DAOCS and by extension, productive O_2 activation by nonheme iron enzymes in general proceed through a concerted mechanism (Scheme 1*B*).

Results

Interaction of αKG and Penicillin-G with Fe^{II}/DAOCS: Availability of a Five-Coordinate Fe^{II}/αKG Site. In order to evaluate the sequential mechanism, the coordination of the Fe^{II} site in DAOCS and its interactions with αKG and penicillin-G substrate were first defined by MCD spectroscopy. Low-temperature MCD spectroscopy in the near-infrared region (Fig. 1 with the corresponding circular dichroism spectra in *SI Appendix*, Fig. S1) probes the Fe^{II} ligand-field transition energies and splitting that enable determination of coordination number and geometry (8). Fe^{II}-DAOCS has two transitions at ~10,000 cm^{-1} split by 1,800 cm^{-1} (Fig. 1, blue), which are diagnostic of a six-coordinate Fe^{II} site. Addition of penicillin-G resulted in only small spectral perturbations (Fig. 1, green), including a small (~100-cm^{-1}) red shift of the ligand-field transitions, a change in their intensity ratio, and a change in the ground-state splitting (from variable-temperature, variable-field MCD of these transitions) (*SI Appendix*, Fig. S2). These small changes indicate that penicillin-G does not directly coordinate to the Fe^{II} and that binding in the active site pocket only modestly perturbs the six-coordinate Fe^{II} center. These small coordination changes are consistent with the substrate binding mode observed in other αKG-dependent enzymes (14–16), in contrast to the

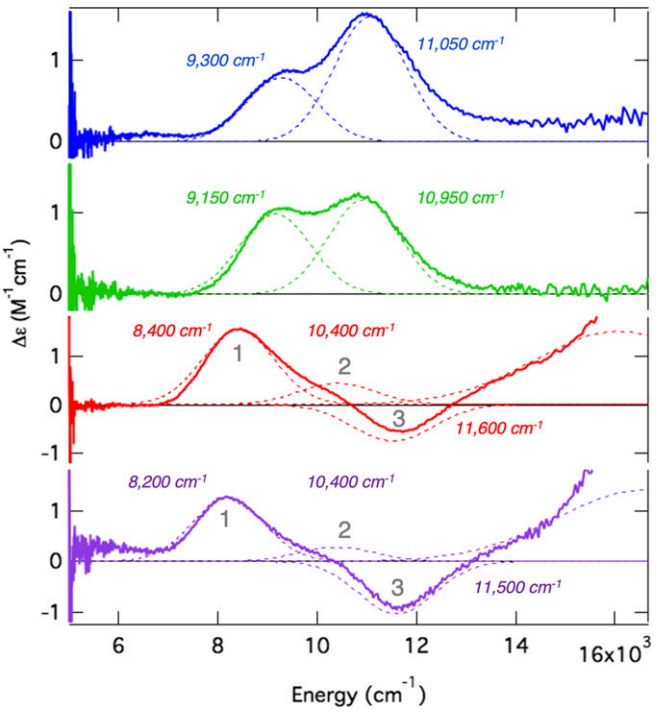

Fig. 1. The 7-T, 5-K MCD spectra for Fe^{II}-DAOCS (blue), (Fe^{II}/penicillin-G [penG])-DAOCS (green), (Fe^{II}/αKG)-DAOCS (red), and (Fe^{II}/αKG/penG)-DAOCS (purple) with Gaussian resolutions and transition energies indicated. In the (Fe^{II}/αKG)-DAOCS (red) and (Fe^{II}/αKG/penG)-DAOCS spectra, the presence of three bands are indicated (numbered 1–3).

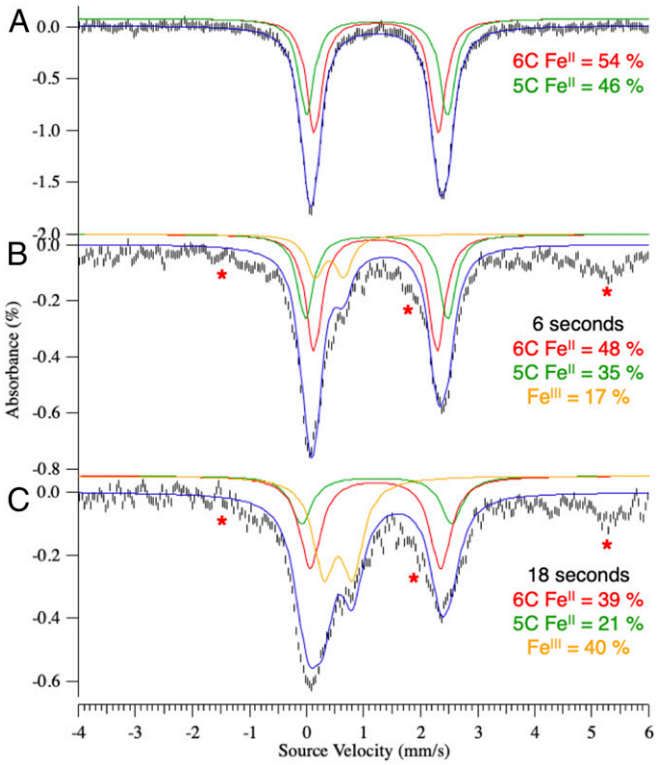

Fig. 2. The 6-K Mössbauer spectra of Fe^{II}-DAOCS/αKG (*A*) reacted with one equivalent O_2 and freeze quenched at 6 s (*B*) and 18 s (*C*). Note that the red asterisks indicate the hyperfine feature associated with a small (<15%) noncatalytic Fe^{III} species, which results from the rapid freeze quench. *SI Appendix, Reaction of Five- and Six-Coordinate (Fe^{II}/αKG)-DAOCS with O_2* and Fig. S9 have details.

crystallographic results that showed penicillin-G coordinating to the Fe^{II} (25).

Addition of αKG to Fe^{II}-DAOCS dramatically changes the MCD spectrum (Fig. 1, red), showing two positive transitions (8,400 and 10,400 cm^{-1}) and a negative transition at higher energy (11,500 cm^{-1}). Furthermore, MCD spectroscopy in the visible energy region revealed an Fe^{II}-to-αKG charge transfer transition (*SI Appendix*, Fig. S3), confirming bidentate αKG binding to the Fe^{II} as observed in other αKG-dependent enzymes (12, 15, 16, 35–37). Since a single Fe^{II} site can only have two ligand-field transitions in the near-infrared spectral region (8), the presence of three bands reflects a mixture of two distinct αKG-bound Fe^{II} centers. Previously studied αKG-bound Fe^{II} active sites show only a single six-coordinate site, in contrast to the Fe^{II}/αKG site in DAOCS (11–13, 36). Additionally, most high-spin Fe^{II} sites studied show all MCD transitions with positive intensity (*SI Appendix, Deviation from the Sum Rule in Fe^{II} MCD Spectroscopy*); negatively signed transitions have only been observed in five-coordinate model complexes and the five-coordinate site of an extradiol dioxygenase (38–40).

Addition of penicillin-G to the αKG-bound Fe^{II} site perturbs the MCD spectrum (Fig. 1, purple), where positive bands 1 and 2 decreased in intensity while the negative intensity of band 3 increased. The presence of the Fe^{II}-to-αKG charge transfer transition (*SI Appendix*, Fig. S3) confirms that αKG is still coordinated bidentate to the Fe^{II} center. Small changes in the ground-state splitting from variable-temperature, variable-field MCD confirm that penicillin-G only slightly perturbs the Fe^{II}/αKG site (*SI Appendix*, Fig. S2), consistent with penicillin-G binding in the active site pocket and not directly to the Fe^{II}. These results demonstrate that simultaneous binding of both αKG and penicillin-G occurs in DAOCS in contrast to the crystallographic results but consistent with the mass spectrometry (25). Furthermore, the intensity changes in the Fe^{II} ligand-field MCD transitions indicate that substrate binding has shifted the ratio of the two species observed in the only αKG-bound mixture, decreasing the component associated with the two positive transitions and increasing the component associated with the negative transition.

In other αKG-dependent enzymes, binding of both αKG and substrate has been found to open a coordination position on the Fe^{II} for O_2 activation (13, 35, 36). In DAOCS, the MCD data above show that substrate binding to the αKG-bound Fe^{II} site increases the component of the mixture associated with the negative transition. Mössbauer spectroscopy of (Fe^{II}/αKG)-DAOCS also shows two ferrous components (δ_1 = 1.22 mm/s, $\Delta E_{Q,1}$ = 2.17 mm/s; δ_2 = 1.24 mm/s, $\Delta E_{Q,2}$ = 2.47 mm/s in Fig. 2*A*). On substrate binding to the αKG bound Fe^{II} site, the species with a larger ΔE_Q increases from 46 to 59% of total Fe^{II} concentration (*SI Appendix*, Fig. S4 and Table S1). Furthermore, X-ray absorption spectroscopy showed that, compared with resting Fe^{II}-DAOCS (which is six coordinate), simultaneous substrate and αKG binding produced a significant five-coordinate contribution (*SI Appendix*, Figs. S5–S8

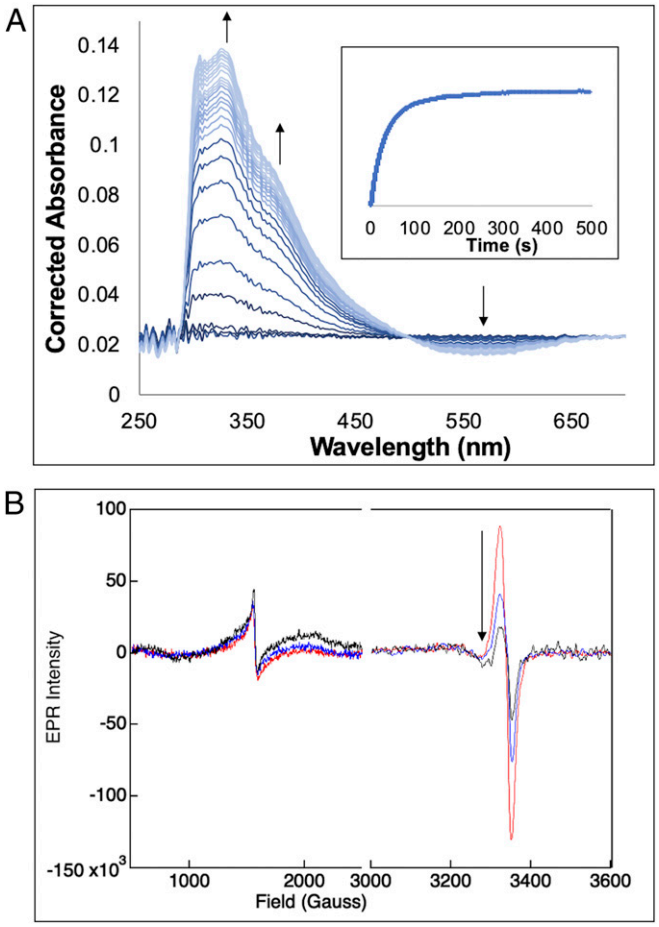

Fig. 3. (*A*) Absorption spectra collected at 5 °C after equal volume mixing of a solution of 0.2 mM DAOCS, 0.2 mM Fe^{II}, and 0.2 mM αKG in 50 mM HEPES buffer, pH 7.5, with O_2-saturated buffer (~2 mM). The spectra were generated by subtracting the spectrum of the DAOCS/αKG mixed with O_2-free buffer. The arrows indicate the appearance of the 335- and 380-nm features with the concurrent disappearance of the 520-nm feature. (*Inset*) Kinetic trace shows the growth of the absorbance at 380 nm. (*B*) Reaction of a solution of 0.2 mM DAOCS, 0.2 mM Fe^{II}, and 0.2 mM αKG in 50 mM HEPES buffer, pH 7.5, with O_2-saturated buffer (~2 mM) monitored EPR spectroscopy with samples frozen at 45 s (red), 100 s (blue), and 6 min (black). The black arrow shows the decay of the g ~ 2 species.

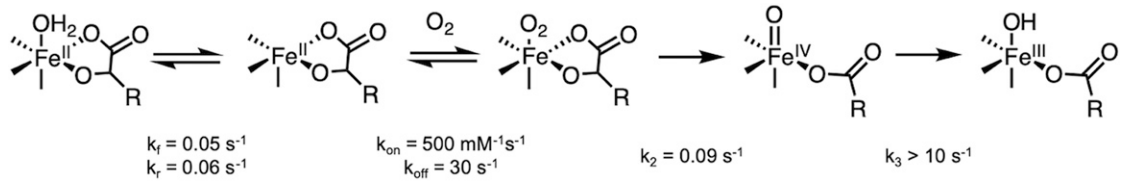

Scheme 2. Kinetic model and corresponding rate parameters used to simulate the stopped-flow data of the reaction of (Fe^{II}/αKG)-DAOCS with O_2.

and Tables S2–S7). Thus, the negative transition in MCD and the Mössbauer doublet with the larger ΔE_Q (δ = 1.24 mm/s, ΔE_Q = 2.47 mm/s) present in (Fe^{II}/αKG)-DAOCS are associated with a five-coordinate site that is also present to a greater (59%) extent in the (Fe^{II}/αKG/penicillin-G)-DAOCS sample. In contrast to other αKG-bound Fe^{II} active sites that are six-coordinate, the presence of this five-coordinate, therefore coordinatively unsaturated, (Fe^{II}/αKG)-DAOCS site allows for the evaluation of the sequential O_2 activation mechanism (Scheme 1*A*) proposed (25) for DAOCS and other αKG-dependent enzymes (25–27).

Reaction of Five- and Six-Coordinate (DAOCS)Fe^{II}/αKG with O_2. From the above MCD results, when only αKG is bound to Fe^{II}-DAOCS, both five- and six-coordinate sites are present. Since the two electron equivalents of the αKG cofactor are available for O_2 reduction, this enabled us to evaluate the relative reactivity of the five- and six-coordinate Fe^{II} sites and the nature of the species generated in this reaction. Starting from Mössbauer spectrum of the anaerobic Fe^{II}/αKG sample (Fig. 2*A*), reaction with O_2 led to the formation of a new Mössbauer doublet (Fig. 2*B*, orange) within 6 s with δ = 0.43 mm/s and ΔE_Q = 0.50 mm/s, consistent with a high-spin Fe^{III} species (*SI Appendix*, *Reaction of Five- and Six-Coordinate (Fe^{II}/αKG)-DAOCS with O_2* and Figs. S9 and S10 have a description of the additional [less than 15%] hyperfine high-spin Fe^{III} signals associated with nonreducible sites). Associated with the formation of the Fe^{III} species in the Mössbauer spectrum, stopped-flow absorption spectra show the growth of two features at 335 and 380 nm (Fig. 3*A*) concomitant with loss of intensity at 520 nm. From the time course of the Mössbauer data in Fig. 2, the five-coordinate component converts to the Fe^{III} site more rapidly than the six-coordinate component. After 6 s, the six-coordinate component has only decreased by 6% of total iron concentration, while the five-coordinate component has decreased by 11%, which together result in 17% Fe^{III} sites. At longer times (>100 s) (*SI Appendix*, Figs. S9–S11), both the Fe^{II} doublets have converted to the Fe^{III} signal.

The Mössbauer Fe^{II} speciation and the kinetics observed from absorption spectroscopy (Fig. 3 *A*, *Inset*) cannot be simultaneously fit with two parallel five-coordinate and six-coordinate Fe^{II} dioxygen reactions. From the Mössbauer data, since the six-coordinate component decays at a slower rate than the five-coordinate component, it converts to the five-coordinate site, which then reacts with O_2. The formation of the 380-nm absorption (Fig. 3 *A*, *Inset*) can be fit with a second-order rate constant of 0.09 $mM^{-1}s^{-1}$ (*SI Appendix*, Fig. S12) (which corresponds to a pseudo first-order rate of 0.09 s^{-1}) and reflects the reaction of the five-coordinate component with O_2 along with an equilibrium six- to five-coordinate Fe^{II} conversion necessary for the O_2 reaction (*SI Appendix*, Fig. S12). The above results show that the five-coordinate Fe^{II} selectively reacts with O_2 and that the slower rate for the six-coordinate component (k_f = 0.05 s^{-1}) reflects loss of H_2O (stabilized in the active site through hydrogen bonds) to enable the O_2 reaction.

Characterization of the Fe^{III} Species and Its Reactivity: Evaluation of the Sequential Mechanism. The appearance of the high-spin Fe^{III} species from Mössbauer spectroscopy (Fig. 2 *B* and *C*) correlates with the growth of the 335/380-nm species from absorption spectroscopy (Fig. 3*A*). In parallel, electron paramagnetic resonance (EPR) spectra reveal the growth of a g′ ∼ 4.3 high-spin Fe^{III} feature and a g ∼ 2.0 S = 1/2 radical feature (Fig. 3*B*). While the ferric g′ ∼ 4.3 species grows and levels off (paralleling the 380-nm absorption and the Fe^{III} Mössbauer doublet), the S = 1/2 radical decays with a rate of 0.02 s^{-1}. The molar absorptivities of the 335- and 380-nm bands (ε_{335} = 3,400 $M^{-1}cm^{-1}$ and ε_{380} = 2,000 $M^{-1}cm^{-1}$) are consistent with ligand-to-metal charge transfer transitions in high-spin Fe^{III} complexes and from the data in *SI Appendix*, Fig. S13, reflect a succinate-bound Fe^{III} site. Furthermore, the loss of intensity at 520 nm in Fig. 3*A* indicates the loss of the Fe^{II}-to-αKG charge transfer in the formation of the Fe^{III} species (note the isosbestic point) and requires that the αKG cofactor has decarboxylated to a succinate. This decarboxylation provides two electrons, and based on the behavior of other αKG-dependent Fe^{II} enzymes (41–44), the Fe^{II} would provide two more electrons to form an Fe^{IV}=O intermediate. The observation of the formation of an Fe^{III} and an organic radical suggests that this ferryl intermediate rapidly decays by H-atom abstraction (or electron and proton transfer) to form an Fe^{III}-OH, which would exhibit the 380- and 335-nm transitions (*SI Appendix*, Figs. S13–S15). It should be noted that further addition of αKG to this Fe^{III}-succinate species reduces it to Fe^{II}, enabling multiple turnovers with O_2 (*SI Appendix*, Figs. S16–S18), which explains the observed decay of the 380-nm species in a similar experiment done in excess αKG where this species was incorrectly assigned as an Fe^{IV}=O intermediate (*SI Appendix*, Fig. S19) (31).

From studies on the αKG- (45) and pterin-dependent hydroxylases (46), the O_2 binding step is fast and reversible relative to the succeeding chemical transformation steps. Due to the lack of a characteristic Fe^{IV}=O absorption (Fig. 3*A*) and Mössbauer features (Fig. 2), the ferryl-oxo species does not measurably accumulate (<5%) prior to formation of the Fe^{III}-succinate/hydroxo species. Fitting the absorption data in Fig. 3 *A*, *Inset* to the kinetic model in Scheme 2 showed that Fe^{IV}=O decay (k_3 > 10 s^{-1}) has to be at least two orders of magnitude faster than its formation (k_2 = 0.09 s^{-1}), reflecting its lack of accumulation.

When the Fe^{III}-succinate/hydroxo species [produced in the O_2 reaction of (Fe^{II}/αKG)-DAOCS] is reacted with penicillin-G substrate, it formed an Fe^{II} species and a species with an EPR signal with g ∼ 2.08 (*SI Appendix*, Figs. S20–S22), consistent with a sulfur-based radical on the penicillin-G substrate (corroborated by electronic structure calculations) (*SI Appendix*, Fig. S22) and with no cephalosporin product formation. Thus, the Fe^{III} produced in the reaction of five-coordinate (DAOCS)Fe^{II}/αKG with O_2 is not competent in product formation, and the Fe^{IV}=O that would form prior to the Fe^{III} species decays at a much faster rate than its formation (Scheme 2), making it inaccessible in a sequential mechanism. These results eliminate a sequential mechanism for DAOCS, consistent with other αKG nonheme iron enzymes (10).

Reactivity of the Fe^{II}/αKG/Penicillin-G Site with O_2: Coupled Turnover via the Concerted Mechanism. Since the sequential mechanism does not produce the cephalosporin product, the reaction of Fe^{II}-DAOCS with both αKG and penicillin-G bound with O_2 was evaluated. Within the first 25 s of the reaction (Fig. 4*A*), an

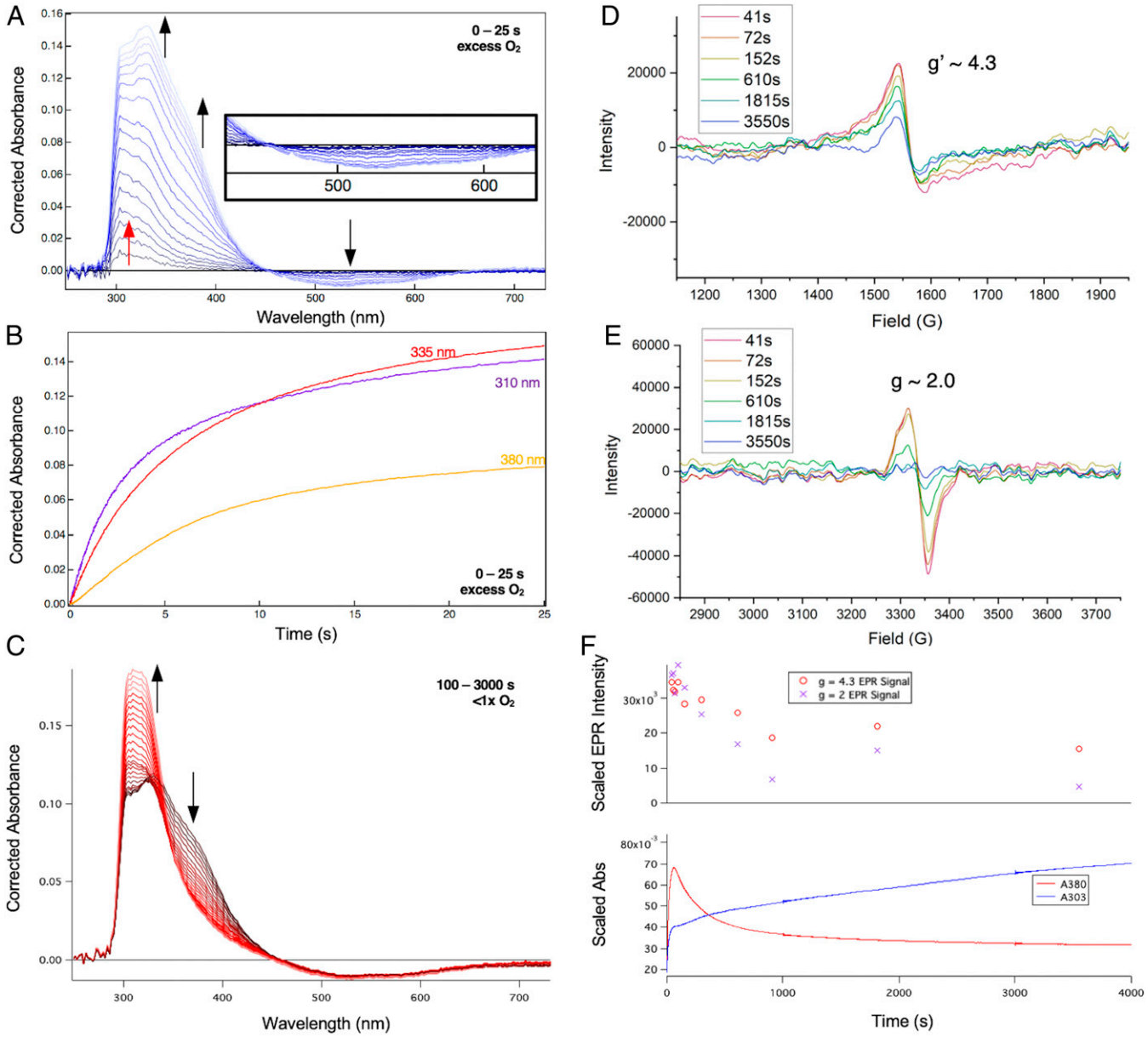

Fig. 4. (*A*) Absorption spectra collected at 5 °C after equal volume mixing of a solution of 0.26 mM DAOCS, 0.26 mM Fe^{II}, 8 mM penicillin-G (penG), and 0.26 mM αKG in 50 mM HEPES buffer, pH 7.5, with O_2-saturated buffer (~2 mM), with the spectrum of DAOCS/αKG/penG mixed with O_2-free buffer subtracted. The red arrow indicates initial growth of the 310-nm feature (expanded in *SI Appendix*, Fig. S18) and the black arrows demonstrate the subsequent disappearance of the 520-nm feature concomitant with the growth of the 335- and 380-nm features. (*Inset*) Expanded view of the 500-nm region. (*B*) Kinetic traces for the experiment in *A* showing absorbances at 310 nm (purple), 335 nm (red), and 380 nm (yellow). (*C*) Same experiment as in *A* and *B* but mixed with 0.2 mM O_2 in buffer, with the spectrum of DAOCS/αKG/penG mixed with O_2-free buffer subtracted. The arrows demonstrate the loss of the 380-nm feature along with the growth of the 303-nm feature. (*D* and *E*) EPR samples frozen at different times along the experiment described in *C*, with the g′ ~ 4.3 region in *D* and the g ~ 2 region in *E*; signals were measured at 77 K. (*F*) Intensity of the g′ ~ 4.3 (*Upper*; red circles) and g ~ 2 (*Upper*; purple crosses) EPR plotted with the absorption time traces of the reaction; monitoring was at 303 nm (*Lower*; blue) and 380 nm (*Lower*; red). The g′ = 4.3 (red circles) EPR signal and the 380-nm time trace (red) do not completely decay due to a minor contribution of the uncoupled (DAOCS)-Fe^{II}/αKG + O_2 reaction described due to poor penG binding [K_M(penG) = 2 mM and (penG) = 8 mM limited by its solubility in the reaction conditions] (54).

absorption feature grows at 310 nm (red arrow in Fig. 4*A* and *SI Appendix*, Fig. S23) followed by the growth of 335- and 380-nm features (black arrows in Fig. 4*A*), apparent in the time traces (Fig. 4*B*). During the growth of the 310-nm species, the intensity at 520 nm is unchanged (dark blue traces in Fig. 4 *A*, *Inset*) but decreases with an isosbestic point at 450 nm as the 335- and 380-nm features subsequently grow in (lighter traces in Fig. 4*A*). Although the 310-nm species does not accumulate enough for Mössbauer characterization, it can be assigned as an Fe^{IV}=O based on its absorption maximum (310 to 320 nm for Fe^{IV}=O in the literature) and the observed lag in decay of spectral features in the 500-nm region (due to growth of Fe^{IV}=O ligand-to-metal charge transfer transitions that overlap the decay of the Fe^{II}-to-αKG charge transfer) (19). The 335/380-nm intermediate is the Fe^{III}-succinate/hydroxo species based on its assignment in the previous section. At later times (under substoichiometric O_2 concentrations, 100 to 3,000 s) (Fig. 4*C*), there is a decrease in intensity in the 335- to 380-nm region, concomitant with the

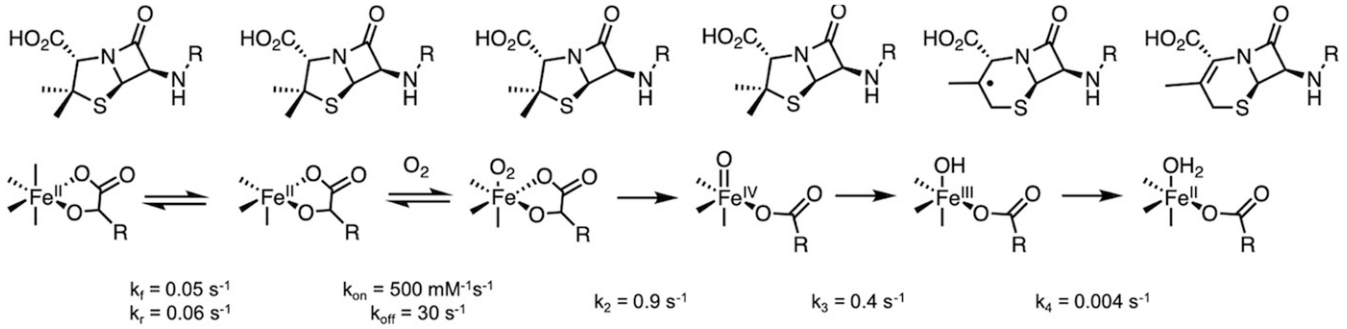

Scheme 3. Kinetic model and corresponding rate parameters used to simulate the stopped-flow data of the reaction of (Fe^{II}/αKG/penicillin-G)-DAOCS with O_2. Since there are 41% six-coordinate sites from Mössbauer, the observed (*SI Appendix*, Fig. S9) six- to five-coordinate conversion rate from Scheme 2 was used to generate the five-coordinate Fe^{II} site that binds O_2.

appearance of an intense 303-nm absorbance feature. This broad, intense 303-nm feature corresponds to the cephalosporin product, with the final product spectrum shown in *SI Appendix*, Fig. S24. Thus, in the presence of bound substrate, the Fe^{III}-succinate/hydroxo species, formed from the reaction of Fe^{IV}=O with substrate, productively forms the cephalosporin product.

EPR samples freeze quenched at different times in the reaction of (Fe^{II}/αKG/penicillin-G)-DAOCS with O_2 show (at 77 K) a g′ ∼ 4.3 signal that correlates with the Fe^{III} absorption feature (Fig. 4*D*) and a radical signal at g ∼ 2 (Fig. 4*E*). From Fig. 4 *D*, g′ ∼ 4.3 and *E*, g ∼ 2, these spectra decay together, which correlates with the formation of the absorption of the cephalosporin product (Fig. 4*F*). When EPR spectra were collected at 5 K, there is an additional resonance at g′ ∼ 7.5 that forms and decays with the g′ ∼ 4.3 and 2.0 signals and is characterized in *SI Appendix*, Fig. S25. In mechanistic proposals for DAOCS, the primary methyl radical rearranges to become a thiyl radical and then, a tertiary radical following ring expansion (Scheme 1*C*). The g value of the radical species in Fig. 4*E* (∼2.0) is consistent with a carbon- rather than thiyl-centered radical (47, 48) and is also distinct from the radical formed in the reaction of (Fe^{II}/αKG)-DAOCS with O_2 as well as the radical of the one-electron oxidized penicillin-G substrate (*SI Appendix*, Fig. S26).

The kinetics of the reaction of Fe^{II}/αKG/penicillin-G with O_2 (Fig. 4) were fit to the model in Scheme 3. In comparing the reaction in the absence and presence of substrate, the addition of substrate increases the rate of Fe^{IV}=O formation by an order of magnitude (k_2 = 0.9 vs. 0.09 s^{-1} without substrate) (Scheme 2). This rate difference is an important finding and indicates that substrate binding to the αKG-bound site activates the site for a more efficient reaction with O_2. Interestingly, the rate of Fe^{IV}=O decay in the substrate-bound reaction is at least an order of magnitude slower (k_3 = 0.4 s^{-1} in Scheme 3) than the Fe^{IV}=O decay rate observed in the substrate-free reaction (k_3 > 10 s^{-1}) (Scheme 2). In the presence of substrate, the Fe^{IV}=O performs an H-atom abstraction from the methyl group on the penicillin ring. In the absence of substrate, the electron and proton sources for reduction of the Fe^{IV}=O to Fe^{III}-OH are not known, but the barrier for this step must be lower than for the difficult C–H bond activation for the substrate (bond dissociation enthalpy [BDE] of the β-methyl group = 99 kcal/mol) (*SI Appendix*, Table S8) and can no longer be accessible when substrate is bound. Furthermore, the Fe^{III} species, formed after Fe^{IV}=O decay in the presence of substrate, is capable of abstracting a second H-atom from the substrate (that it is now a radical with a BDE = 36 kcal/mol) (*SI Appendix*, Table S8) to form the ring-expanded product. Thus, while the Fe^{III}OH/succinate cannot perform H-atom abstraction from the substrate in a sequential mechanism, it can on the substrate radical in the concerted mechanism, confirming the latter mechanism for αKG-dependent Fe^{II} enzyme catalysis.

Discussion

This study provides important insight into the mechanism of αKG-dependent nonheme iron enzyme catalysis using DAOCS, for which past results have been controversial. Variable-temperature, variable-field MCD spectroscopy showed that both cosubstrates can simultaneously bind to the Fe^{II} active site and that penicillin-G substrate does not directly bind to the metal center (14–16, 25) and behaves similarly to other enzymes in this family. However, unlike other members of this family, the αKG only-bound site in DAOCS does have a five-coordinate component as demonstrated by variable-temperature, variable-field MCD, Mössbauer, and X-ray absorption spectroscopies. The five-coordinate Fe^{II} site selectively reacts with O_2 from the Mössbauer data (Fig. 2), while the six-coordinate component reacts slower, likely reflecting the rate of loss of a water ligand to form the reactive five-coordinate Fe^{II} site.

The presence of a five-coordinate component when only αKG is bound enabled evaluation of a sequential mechanism. As summarized in Scheme 4, reaction of the five-coordinate Fe^{II}/αKG site with O_2 forms a stable HO-Fe^{III}-succinate species and not an Fe^{II}-peroxy-succinate that had been predicted through crystallography and electronic structure calculations (25). Reaction of this Fe^{III} species with penicillin-G substrate results in unproductive one-electron oxidation of penicillin-G. The Fe^{IV}=O, which would produce this Fe^{III} species by reaction with a protein residue in the absence of substrate, is formed slowly and dissipates

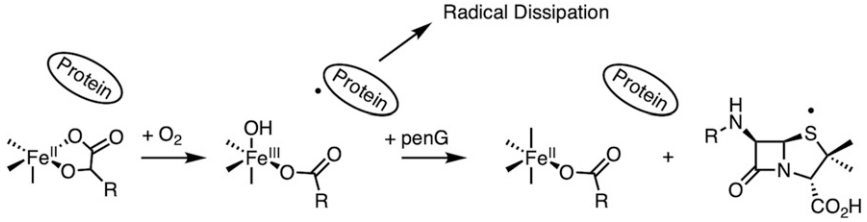

Scheme 4. Uncoupled reactivity of DAOCS. Note that penG refers to the penicillin-G substrate.

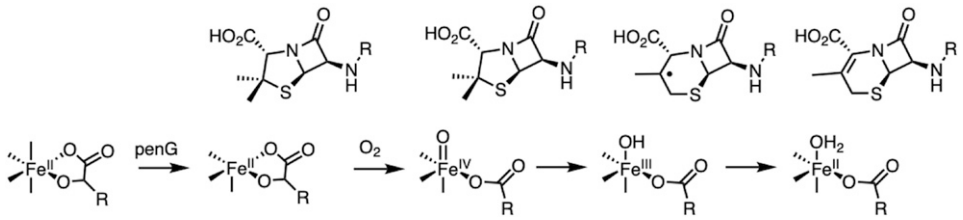

Scheme 5. General mechanistic strategy in DAOCS. Note that penG refers to the penicillin-G substrate.

rapidly, making it kinetically inaccessible. Thus, the sequential mechanism (Scheme 1*A*) is not operative for productive chemistry in αKG-dependent Fe enzymes.

As shown in Scheme 5, the concerted mechanism was evaluated by reacting the Fe^{II}/αKG/penicillin-G site with O_2. An Fe^{IV}=O species first forms but rapidly decays to an Fe^{III}-succinate species along with the substrate radical. Note that this species is an Fe^{III}-OH and not an Fe^{III}-oxo species [previously proposed in αKG-dependent enzyme catalysis (49)] based on its small ΔE_Q splitting from Mössbauer spectroscopy and rhombic EPR signal as observed in Fe^{III}-OH (but not Fe^{III}-oxo) model complex chemistry (50, 51). Proceeding from the Fe^{III}-OH intermediate and substrate radical, unlike the behavior observed in the uncoupled reaction (i.e., no substrate) (Scheme 4), both the ferric species and the organic radical decay together and productively to form the cephalosporin product. Thus, the binding of the penicillin-G substrate to the Fe^{II}/αKG site before reaction with O_2 is required for productive turnover, demonstrating that the concerted mechanism is operative in DAOCS. In the concerted pathway, from EPR spectroscopy one dominant g ∼ 2 radical species is observed. From mechanistic proposals for DAOCS, the primary methyl group in penicillin substrates undergoes H-atom abstraction and then, rearranges to a tertiary radical by C–S bond scission through a putative thiyl radical from stereochemical studies (34). Since the interconversion of these species is not observed, this rearrangement must be rapid: at least an order of magnitude faster than the H-atom abstraction by the Fe^{IV}=O. Furthermore, since there is no evidence for primary hydroxylation, the rapid rearrangement of the radical would provide a mechanism to suppress hydroxylation reactivity in the αKG-dependent hydroxylases, similar to a proposal in the literature (52).

In the concerted mechanism, the O_2 reaction to form an Fe^{IV}=O is an order of magnitude faster than in the absence of substrate. This rate difference has two main contributions: 1) electronic, where the substrate- and cofactor-bound Fe^{II} site has a more activated dπ orbital, and 2) steric, where clash between the substrate and the sixth water ligand leads to five-coordinate conversion, both of which prime the active site for efficient O_2 activation (13, 53). In the concerted reaction, the formation of cephalosporin (i.e., the second H-atom abstraction by the Fe^{III}-OH from the substrate radical) is rate limiting, which is likely due to the poor orientation of the rearranged penicillin-G substrate radical in the DAOCS active site. Finally, the substrate radical decays more than an order of magnitude slower than the protein residue radical (in the absence of substrate), indicating that, in the presence of substrate, autooxidation is inaccessible, likely due to substrate positioning preventing electron/proton transfer from the protein residue to the Fe^{IV}=O intermediate.

This study has shown that the general mechanistic strategy, where both cosubstrates are bound to the active site to generate a five-coordinate Fe^{II} for O_2 activation, is an effective gating mechanism that is required by nonheme iron enzymes for productive catalysis.

Materials and Methods

Details about protein expression and purification, sample preparation, spectroscopic methods, X-ray absorption experiments and data analysis, stopped-flow absorption experiments, and kinetic simulations are provided in *SI Appendix, Materials and Methods*.

Data Availability. All data are included in the manuscript or *SI Appendix*.

ACKNOWLEDGMENTS. This research was supported by the US NIH Grant GM 40392 (to E.I.S.). Use of the Stanford Synchrotron Radiation Lightsource, SLAC National Accelerator Laboratory is supported by US Department of Energy, Office of Science, Office of Basic Energy Sciences Contract DE-AC02-76SF00515. The Stanford Synchrotron Radiation Lightsource (SSRL) Structural Molecular Biology Program is supported by the Department of Energy Office of Biological and Environmental Research and by NIH, National Institute of General Medical Sciences Grant P41GM103393 (to B.H. and K.O.H.). G.H.J.P. acknowledges funding from Independent Research Fund Denmark Grant DFF-6108-00247. We thank Dr. Leland B. Gee for helpful discussions and analysis of the X-ray absorption data.

1. S. W. Elson *et al.*, The roles of clavaminic acid and proclavaminic acid in clavulanic acid biosynthesis. *J. Chem. Soc. Chem. Commun.* **22**, 1739–1740 (1987).
2. J. E. Baldwin, E. Abraham, The biosynthesis of penicillins and cephalosporins. *Nat. Prod. Rep.* **5**, 129–145 (1988).
3. P. F. Fitzpatrick, Tetrahydropterin-dependent amino acid hydroxylases. *Annu. Rev. Biochem.* **68**, 355–381 (1999).
4. D. Lando *et al.*, FIH-1 is an asparaginyl hydroxylase enzyme that regulates the transcriptional activity of hypoxia-inducible factor. *Genes Dev.* **16**, 1466–1471 (2002).
5. B. G. Keenan, T. K. Wood, Orthric Rieske dioxygenases for degrading mixtures of 2,4-dinitrotoluene/naphthalene and 2-amino-4,6-dinitrotoluene/4-amino-2,6-dinitrotoluene. *Appl. Microbiol. Biotechnol.* **73**, 827–838 (2006).
6. F. H. Vaillancourt *et al.*, Characterization of extradiol dioxygenases from a polychlorinated biphenyl-degrading strain that possess higher specificities for chlorinated metabolites. *J. Bacteriol.* **185**, 1253–1260 (2003).
7. Y. Mishina, C. He, Oxidative dealkylation DNA repair mediated by the mononuclear non-heme iron AlkB proteins. *J. Inorg. Biochem.* **100**, 670–678 (2006).
8. E. I. Solomon *et al.*, Geometric and electronic structure/function correlations in non-heme iron enzymes. *Chem. Rev.* **100**, 235–350 (2000).
9. S. Kal, L. Que, Dioxygen activation by nonheme iron enzymes with the 2-His-1-carboxylate facial triad that generate high-valent oxoiron oxidants. *J. Biol. Inorg. Chem.* **22**, 339–365 (2017).
10. E. I. Solomon, S. Goudarzi, K. D. Sutherlin, O_2 activation by non-heme iron enzymes. *Biochemistry* **55**, 6363–6374 (2016).
11. J. Zhou *et al.*, Spectroscopic studies of substrate interactions with clavaminate synthase 2, a multifunctional α-KG-dependent non-heme iron enzyme: Correlation with mechanisms and reactivities. *J. Am. Chem. Soc.* **123**, 7388–7398 (2001).
12. E. G. Pavel *et al.*, Circular dichroism and magnetic circular dichroism spectroscopic studies of the non-heme ferrous active site in clavaminate synthase and its interaction with α-ketoglutarate cosubstrate. *J. Am. Chem. Soc.* **120**, 743–753 (1998).
13. K. M. Light, J. A. Hangasky, M. J. Knapp, E. I. Solomon, Spectroscopic studies of the mononuclear non-heme $Fe^{(II)}$ enzyme FIH: Second-sphere contributions to reactivity. *J. Am. Chem. Soc.* **135**, 9665–9674 (2013).
14. J. M. Elkins *et al.*, X-ray crystal structure of Escherichia coli taurine/α-ketoglutarate dioxygenase complexed to ferrous iron and substrates. *Biochemistry* **41**, 5185–5192 (2002).
15. J. M. Elkins *et al.*, Structure of factor-inhibiting hypoxia-inducible factor (HIF) reveals mechanism of oxidative modification of HIF-1 alpha. *J. Biol. Chem.* **278**, 1802–1806 (2003).
16. Z. Zhang *et al.*, Structural origins of the selectivity of the trifunctional oxygenase clavaminic acid synthase. *Nat. Struct. Biol.* **7**, 127–133 (2000).
17. E. I. Solomon, K. M. Light, L. V. Liu, M. Srnec, S. D. Wong, Geometric and electronic structure contributions to function in non-heme iron enzymes. *Acc. Chem. Res.* **46**, 2725–2739 (2013).
18. S. Martinez, R. P. Hausinger, Catalytic mechanisms of Fe(II)- and 2-oxoglutarate-dependent oxygenases. *J. Biol. Chem.* **290**, 20702–20711 (2015).
19. J. C. Price, E. W. Barr, B. Tirupati, J. M. Bollinger Jr, C. Krebs, The first direct characterization of a high-valent iron intermediate in the reaction of an α-ketoglutarate-dependent dioxygenase: A high-spin FeIV complex in taurine/α-ketoglutarate dioxygenase (TauD) from Escherichia coli. *Biochemistry* **42**, 7497–7508 (2003).

20. L. M. Hoffart, E. W. Barr, R. B. Guyer, J. M. Bollinger Jr, C. Krebs, Direct spectroscopic detection of a C-H-cleaving high-spin Fe(IV) complex in a prolyl-4-hydroxylase. *Proc. Natl. Acad. Sci. U.S.A.* **103**, 14738–14743 (2006).
21. M. L. Matthews *et al*., Substrate-triggered formation and remarkable stability of the C-H bond-cleaving chloroferryl intermediate in the aliphatic halogenase, SyrB2. *Biochemistry* **48**, 4331–4343 (2009).
22. D. G. Fujimori *et al*., Spectroscopic evidence for a high-spin Br-Fe(IV)-oxo intermediate in the α-ketoglutarate-dependent halogenase CytC3 from Streptomyces. *J. Am. Chem. Soc.* **129**, 13408–13409 (2007).
23. N. P. Dunham *et al*., Two distinct mechanisms for C-C desaturation by iron(II)- and 2-(Oxo)glutarate-dependent oxygenases: Importance of α-heteroatom assistance. *J. Am. Chem. Soc.* **140**, 7116–7126 (2018).
24. N. P. Dunham *et al*., α-Amine desaturation of **d**-arginine by the iron(II)- and 2-(Oxo) glutarate-dependent **l**-arginine 3-hydroxylase, vioC. *Biochemistry* **57**, 6479–6488 (2018).
25. K. Valegård *et al*., The structural basis of cephalosporin formation in a mononuclear ferrous enzyme. *Nat. Struct. Mol. Biol.* **11**, 95–101 (2004).
26. N. C. Giri, H. Sun, H. Chen, M. Costa, M. J. Maroney, X-ray absorption spectroscopy structural investigation of early intermediates in the mechanism of DNA repair by human ABH2. *Biochemistry* **50**, 5067–5076 (2011).
27. L. J. Higgins, F. Yan, P. Liu, H. W. Liu, C. L. Drennan, Structural insight into antibiotic fosfomycin biosynthesis by a mononuclear iron enzyme. *Nature* **437**, 838–844 (2005).
28. R. B. Hamed *et al*., The enzymes of β-lactam biosynthesis. *Nat. Prod. Rep.* **30**, 21–107 (2013).
29. J. E. Dotzlaf, W. K. Yeh, Copurification and characterization of deacetoxycephalosporin C synthetase/hydroxylase from Cephalosporium acremonium. *J. Bacteriol.* **169**, 1611–1618 (1987).
30. A. Dubus *et al*., Probing the penicillin sidechain selectivity of recombinant deacetoxycephalosporin C synthase. *Cell. Mol. Life Sci.* **58**, 835–843 (2001).
31. H. Tarhonskaya *et al*., Studies on deacetoxycephalosporin C synthase support a consensus mechanism for 2-oxoglutarate dependent oxygenases. *Biochemistry* **53**, 2483–2493 (2014).
32. J. E. Baldwin *et al*., Cephalosporin biosynthesis: A branched pathway sensitive to an isotope effect. *Tetrahedron* **47**, 9881–9900 (1991).
33. H.-J. Lee *et al*., Kinetic and crystallographic studies on deacetoxycephalosporin C synthase (DAOCS). *J. Mol. Biol.* **308**, 937–948 (2001).
34. C. A. Townsend, A. B. Theis, A. S. Neese, E. B. Barrabee, D. Poland, Stereochemical fate of chiral methyl of valine in the ring expansion of penicillin N to deacetoxycephalosporin C. *J. Am. Chem. Soc.* **107**, 4760–4767 (1985).
35. J. Zhou, M. Gunsior, B. O. Bachmann, C. A. Townsend, E. I. Solomon, Substrate binding to the α-ketoglutarate-dependent non-heme iron enzyme clavaminate synthase 2: Coupling mechanism of oxidative decarboxylation and hydroxylation. *J. Am. Chem. Soc.* **120**, 13539–13540 (1998).
36. M. L. Neidig *et al*., CD and MCD of CytC3 and taurine dioxygenase: Role of the facial triad in α-KG-dependent oxygenases. *J. Am. Chem. Soc.* **129**, 14224–14231 (2007).
37. K. Valegård *et al*., Structure of a cephalosporin synthase. *Nature* **394**, 805–809 (1998).
38. E. G. Pavel, N. Kitajima, E. I. Solomon, Magnetic circular dichroism spectroscopic studies of mononuclear non-heme ferrous model complexes. Correlation of excited- and ground-state electronic structure with geometry. *J. Am. Chem. Soc.* **120**, 3949–3962 (1998).
39. P. A. Mabrouk, A. M. Orville, J. D. Lipscomb, E. I. Solomon, Variable-temperature variable-field magnetic circular dichroism studies of the iron(II) active site in metapyrocatechase: Implications for the molecular mechanism of extradiol dioxygenases. *J. Am. Chem. Soc.* **113**, 4053–4061 (1991).
40. M. I. Davis *et al*., Spectroscopic and electronic structure studies of 2,3-dihydroxybiphenyl 1,2-dioxygenase: O_2 reactivity of the non-heme ferrous site in extradiol dioxygenases. *J. Am. Chem. Soc.* **125**, 11214–11227 (2003).
41. M. J. Ryle *et al*., O_2- and α-ketoglutarate-dependent tyrosyl radical formation in TauD, an α-keto acid-dependent non-heme iron dioxygenase. *Biochemistry* **42**, 1854–1862 (2003).
42. T. F. Henshaw, M. Feig, R. P. Hausinger, Aberrant activity of the DNA repair enzyme AlkB. *J. Inorg. Biochem.* **98**, 856–861 (2004).
43. A. Liu *et al*., Alternative reactivity of an α-ketoglutarate-dependent iron(II) oxygenase: Enzyme self-hydroxylation. *J. Am. Chem. Soc.* **123**, 5126–5127 (2001).
44. M. Mantri, Z. Zhang, M. A. McDonough, C. J. Schofield, Autocatalysed oxidative modifications to 2-oxoglutarate dependent oxygenases. *FEBS J.* **279**, 1563–1575 (2012).
45. J. C. Price, E. W. Barr, L. M. Hoffart, C. Krebs, J. M. Bollinger Jr, Kinetic dissection of the catalytic mechanism of taurine:α-ketoglutarate dioxygenase (TauD) from Escherichia coli. *Biochemistry* **44**, 8138–8147 (2005).
46. M. S. Chow *et al*., Spectroscopy and kinetics of wild-type and mutant tyrosine hydroxylase: Mechanistic insight into O_2 activation. *J. Am. Chem. Soc.* **131**, 7685–7698 (2009).
47. B. G. Segal, M. Kaplan, G. K. Fraenkel, Measurement of g values in the electron spin resonance spectra of free radicals. *J. Chem. Phys.* **43**, 4191–4200 (1965).
48. J. J. Windle, A. K. Wiersema, A. L. Tappel, Electron paramagnetic resonance of some sulfur and selenium compounds. *J. Chem. Phys.* **41**, 1996–2002 (1964).
49. P. K. Grzyska, E. H. Appelman, R. P. Hausinger, D. A. Proshlyakov, Insight into the mechanism of an iron dioxygenase by resolution of steps following the FeIV=HO species. *Proc. Natl. Acad. Sci. U.S.A.* **107**, 3982–3987 (2010).
50. C. E. MacBeth *et al*., Utilization of hydrogen bonds to stabilize M-O(H) units: Synthesis and properties of monomeric iron and manganese complexes with terminal oxo and hydroxo ligands. *J. Am. Chem. Soc.* **126**, 2556–2567 (2004).
51. Z. Gordon *et al*., Characterization of terminal iron(III)-Oxo and iron(III)-hydroxo complexes derived from O_2 activation. *Inorg. Chem.* **58**, 15801–15811 (2019).
52. J. Pan *et al*., Evidence for modulation of oxygen rebound rate in control of outcome by iron(II)- and 2-oxoglutarate-dependent oxygenases. *J. Am. Chem. Soc.* **141**, 15153–15165 (2019).
53. S. R. Iyer, V. D. Chaplin, M. J. Knapp, E. I. Solomon, O_2 activation by nonheme Fe^{II} α-ketoglutarate-dependent enzyme variants: Elucidating the role of the facial triad carboxylate in FIH. *J. Am. Chem. Soc.* **140**, 11777–11783 (2018).
54. M. D. Lloyd *et al*., Studies on the active site of deacetoxycephalosporin C synthase. *J. Mol. Biol.* **287**, 943–960 (1999).